

SAOLIM, A PROTOTYPE OF A LOW COST SYSTEM FOR ADAPTIVE OPTICS WITH LUCKY IMAGING. DESIGN AND PERFORMANCE.

J. ACEITUNO AND S. F. SANCHEZ

Centro Astronomico Hispano-Aleman (CAHA), Jesus Durban Remon 2-2, 04004 Almeria, Spain

J. L. ORTIZ AND F. J. ACEITUNO

Instituto de Astrofísica de Andalucía, CSIC Granada, Spain

Draft version November 9, 2018

ABSTRACT

A prototype of a low cost Adaptive Optics (AO) system has been developed at the Instituto de Astrofísica de Andalucía (CSIC) and tested at the 2.2m telescope of the Calar Alto observatory. We present here the status of the project, which includes the image stabilization system and compensation of high order wavefront aberrations with a membrane deformable mirror. The image stabilization system consists of **magnet** driven tip-tilt mirror. The higher order compensation system **comprises** of a Shack-Hartmann sensor, a membrane deformable mirror with 39 actuators and the control computer that allows operations up to 420Hz in closed loop mode. We have successfully closed the high order AO loop on natural guide stars. An improvement of 4 times in terms of FWHM was achieved. The description and the results obtained on the sky are presented in this paper.

Subject headings: Adaptive optics, micromachined membrane deformable mirror, EMCCD, low cost.

1. INTRODUCTION

The use of adaptive optics in astronomy with reasonable spatial order correction and temporal bandwidths has been restricted for many years to observatories with a high instrumentation budget. In current versions, such systems use expensive deformable mirrors, and digital signal processors to apply the reconstruction algorithms. This results in complex systems (e.g. Hippler et al. 2000), taking several years to be developed. Nowadays, the total cost can be reduced by several orders of magnitude (e.g. Dainty et al. 1999) thanks to the availability of relatively cheap membrane deformable mirrors (Vdovin 1995), single photon detectors with a **reasonably** high frame rate based on the EMCCD technology (e.g. Dussault & Hoess 2004) and low cost Tip-Tilt systems.

In this paper we describe a System of Adaptive Optics with Lucky Imaging (hereafter SAOLIM). We present the design, construction and results of a low order AO system for 1-2m class telescopes, almost entirely developed with available commercial components, and with a total cost of ~ 35000 euros in hardware components.

The optical design enables a FOV of 90×90 arcsec² for the scientific camera. SAOLIM is optically corrected and transparent for a wavelength range between 1.0 - $2.5 \mu\text{m}$.

Our system is based on a membrane deformable mirror (e.g. Paterson et al. 2000), and a single PC to perform all the computations and hardware control, integrating everything in a simple and compact design as we will see later. The dual wireless/ethernet communication of the device allows an easy setup, because no cabling has to be installed at the telescope, reducing a considerable amount of possible problems.

This instrument can be used as an input correction for applications where reaching the diffraction limit of the telescope is required, such as a lucky imag-

ing system, like ASTRALUX (Hormuth et al. 2008), or as a complement for the shift-and-add approach (e.g. Bates & Cady 1980). This device can take advantage of a low order AO system, in such a way that the rate of the useful images could be increased, and therefore the performance of the instrument can be improved. Such innovative technique has been tested recently at the Palomar observatory, getting excellent results (e.g. Law et al. 2008).

2. SYSTEM DESCRIPTION

Figure 1 shows a picture of the instrument attached to the telescope. Labels indicating the main components have been included. A detail of the optical components is shown in Figure 2 where a view of the inside of the instrument (located at the lab) is presented. The main optical elements have been labelled in this figure.

2.1. Mechanical and optical design.

A sketch of the optical setup is shown in Figure 3. The optical design is similar to that of ALFA, the AO system that was operated at the 3.5m telescope of the Calar Alto observatory since 1997 until 2005 (e.g. Hippler et al. 2000). A Shack-Hartmann wavefront sensor (hereafter SHS) is placed optically conjugated with the membrane deformable mirror (MDMM) and with the entrance pupil of the whole system. **To align the pupil on the DM, a camera is temporarily located in different parts of the optical axis, until a sharp image of the main mirror is obtained.** Two achromatic doublets (E1) separated by 5mm, with focal distances of 300mm each one conjugate the entrance pupil over a 20mm diameter circular area on the deformable mirror. Another pair of achromatic doublet lenses (E3 and E6) is configured as a Kepler telescope and conjugates the membrane's selected zone on the SHS. The SHS consists of a microlenses array (E7, focal length 45mm) and two achromatic doublet lenses (E8 and E9) to re-

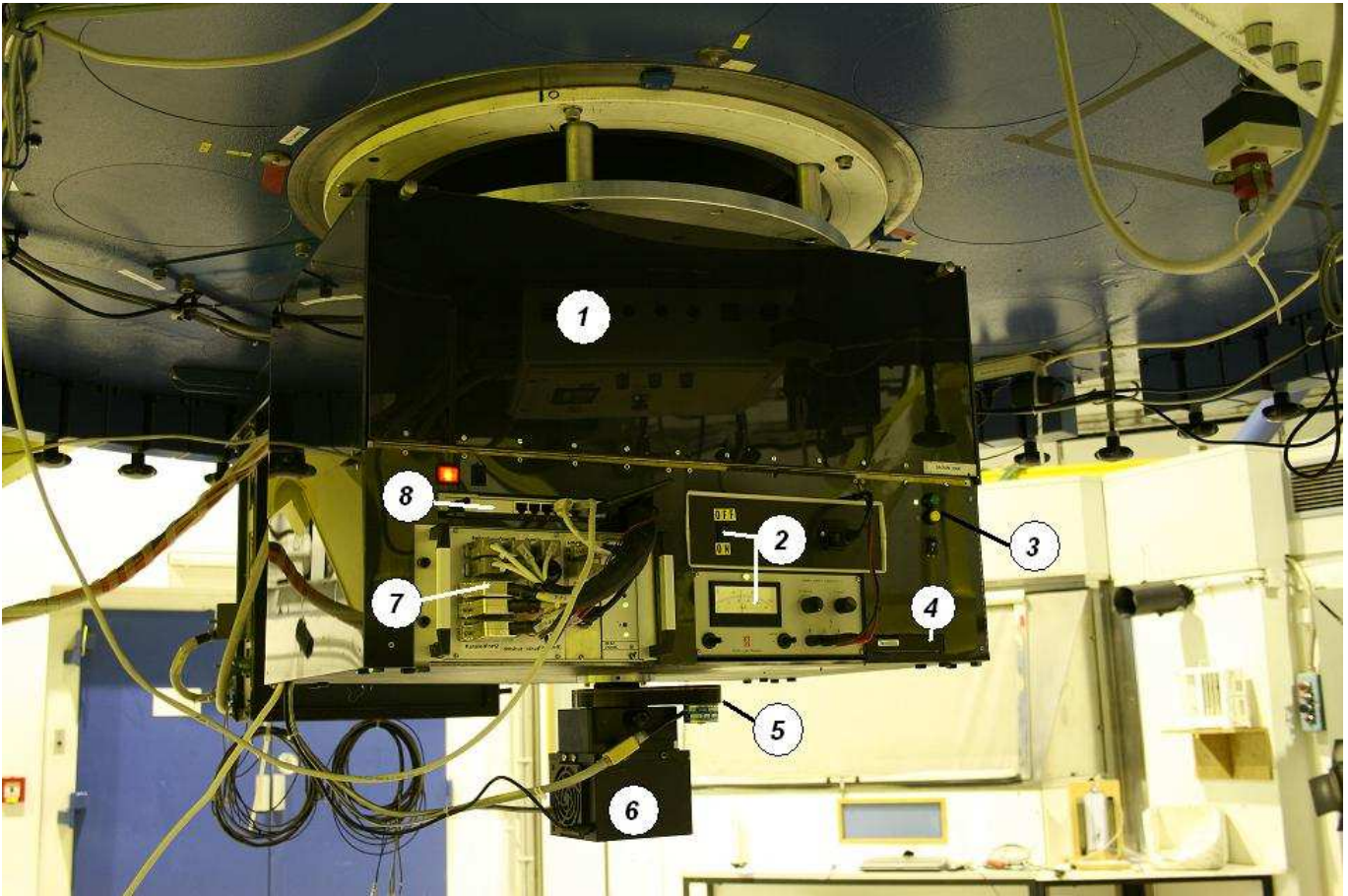


FIG. 1.— SAOLIM mounted at the Calar Alto 2.2m Telescope Cassegrain Focus. Different elements are labeled: (1) Optical bench, (2) DM electronics, (3) PC Pentium IV, (4) hard disk, (5) scientific filter wheel, (6) scientific camera, (7) hardware electronic, (8) router. The instrument measures 75x40x50cm and weights 70kg.

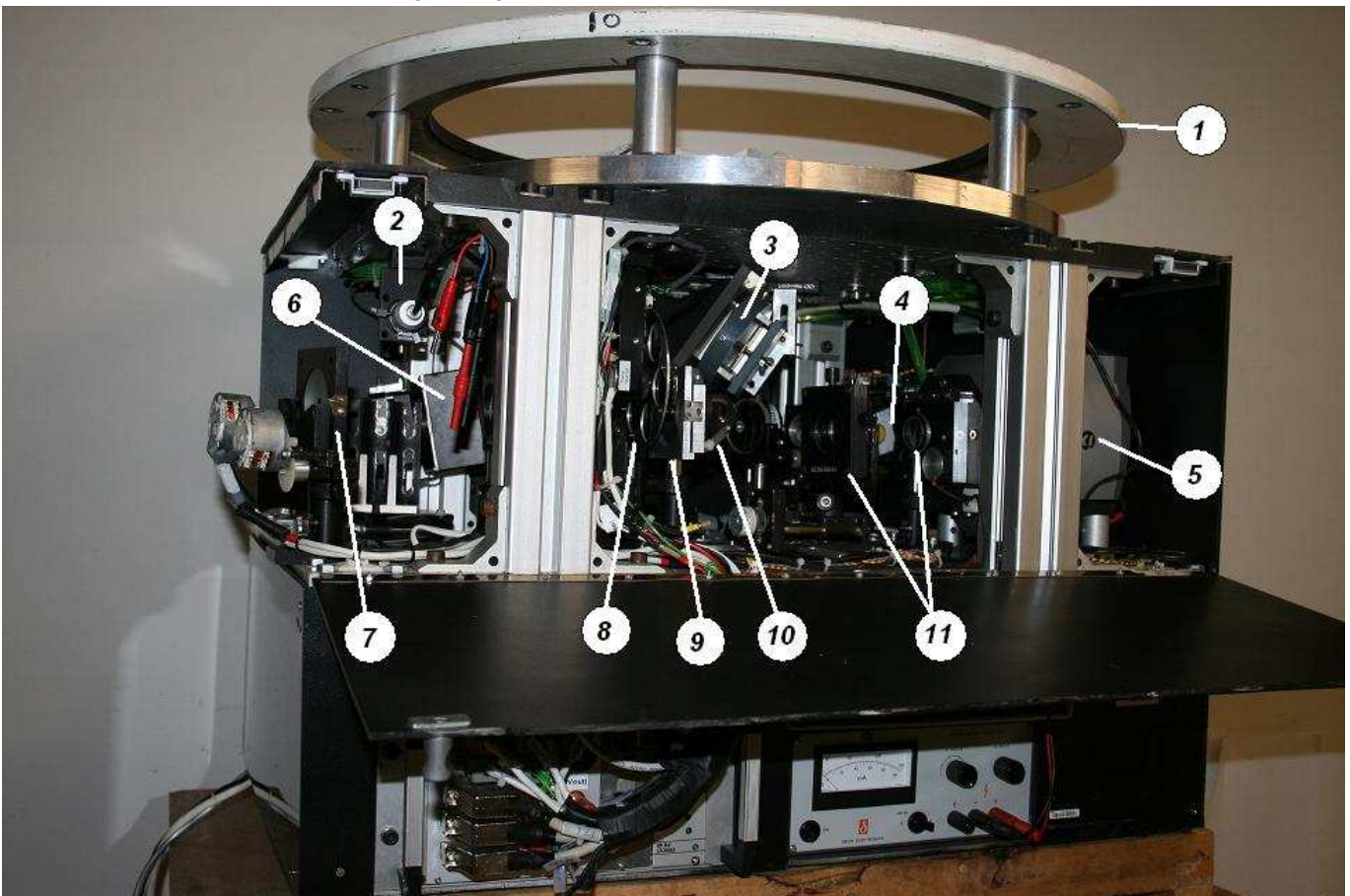


FIG. 2.— Lateral picture of the optical bench in SAOLIM: (1) Cassegrain adapter, (2) a reference fiber located at $f/8$ focus, (3) filter wheel, (4) scientific camera, (5) scientific filter wheel, (6) scientific camera, (7) hardware electronic, (8) router, (9) hard disk, (10) PC Pentium IV, (11) DM electronics.

TABLE 1
MAIN INSTRUMENT PARAMETERS

AO SYSTEM	
focal ratio:	cassegrain f:8
principle of operation:	Adaptive optics system
AO closed-loop sample speed:	420Hz
modes of reconstruction:	15
WAVEFRONT SENSOR	
principle of operation:	Shack-Hartmann sensor
detector:	EMCCD Andor IXON DU860
Chip size:	128x128 pixels
lenslet-arrays:	5x5 ^a and KS28 ^b
pixel scale:	0.45 arcsec/pixel
FOV of each spot:	10.5 arcsec
wavelength range:	400-950 nm
filter wheel:	6 positions. Neutral density filters
DEFORMABLE MIRROR	
principle of operation:	membrane deformable mirror
actuators:	39
diameter:	30mm
maximun depth:	8 μ m ^c
voltage range:	0-250V
sample speed:	1kHz
reference voltage:	180V
Useful diameter:	20mm ^c
TIP-TILT SYSTEM	
principle of operation:	magnetic pivots
model:	AO-7 SBIG
sample speed:	50Hz
SCIENTIFIC CAMERA	
principle of operation:	back-iluminated CCD 1024x1024
scientific camera FOV:	90x90 arcsec ²
pixel scale:	0.08 arcsec/pixel
pixel size:	24 μ m
filter wheel:	4 positions 50mm dia. each
wavelength range:	950-2500 nm
CONTROL	
principle of operation:	Single PC INTEL pentium IV 3.4Ghz, 2Gb RAM

^a5x5 hexagonal microlenses.

^bkeystone-shaped microlenses.

^cAccording to the manufacturer.

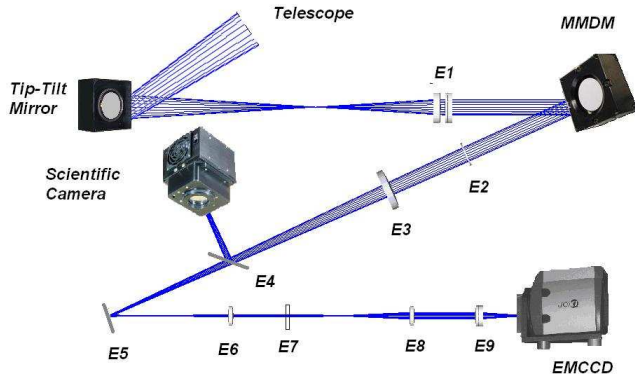


FIG. 3.— The Figure shows the optical design of SAOLIM.

image the subapertures spots on the EMCCD with an appropriate pixel scale yielding a value of $0.48''/\text{pixel}$. An aplanatic lens (E2) is placed between the MMDM and E3 to reduce coma aberration in the Kepler telescope. A dichroic beam-splitter (E4) reflects the near infrared part of the spectrum to the scientific camera whereas the visible part to go to the SHS. Finally, a motorized flat mirror (E5) folds the optical path to keep the design compact.

The optical performance of the design was evaluated with the optical software ZEMAX¹. Figures 4 and 5 show the spots sizes at different field angles at the scientific camera of SAOLIM. The geometry and sizes of the spots are comparable to those of the Airy disk in different angles, whose amplitudes have been selected to match the isoplanatic angle in the K-Band. The Strehl ratio expected is about 72%, close to the theoretical value of 82%, foreseen by ZEMAX. The image quality is almost constant through the different angles, with a wavefront distortion smaller than $\frac{\lambda}{4}$ (Fig 4). The system is equipped with an artificial point source fed by an optical fiber and has other movable motorized components such a filter wheel, shutters, and focuser of the wavefront sensor (WFS, hereafter).

Finally, the Tip-Tilt mirror is located just before the DM. The only drawback of not being located in the pupil plane is that it is moved around the ground-layer turbulence. According to ZEMAX this produces a shift in the science camera's pupil of less than 1% of its size, for a typical atmospheric Tip-Tilt. This wouldn't harm even coronagraphic observations with an under-size stop. On the positive side, at least two optical elements (which would be required to re-image the pupil) are saved. Similar design have been adopted in other working AO systems (e.g. Hippler et al. 2000), (e.g. Peter et al. 2010)

2.2. Wavefront sensor.

The wavefront reflected by the deformable mirror can be sampled by two different lenslet arrays with different configurations. The first one is a keystone-shaped array

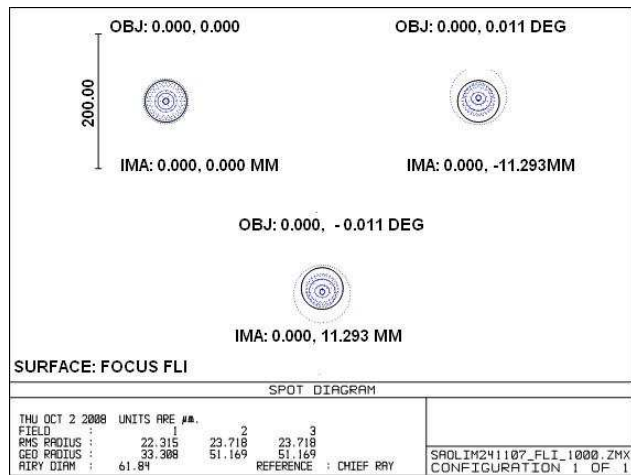


FIG. 4.— Spot geometry at the scientific camera at different entry angles. The field of view is 90 arcseconds. Values estimated by Zemax.

with 28 microlenses (Figure 6) which is detected by a 128x128 pixels EMCCD camera. The focal length of the microlenses is 45mm. This geometry allows for an optimum filling of the annular telescope aperture contrary to other designs, like an hexagonal or square grid. In addition, if the subapertures in the different rings are designed in such a way that all of them have the same area, the spots are equally bright, and the noise pattern is uniform. The reconstruction benefits of this configuration with respect to other more usual ones (e.g. hexagonal-shaped) are described by (Kasper & Hippler 2003).

A second array comprises a 5x5 hexagonal-shaped lens configuration (Figure 6) with a focal length of 36.1mm and 1mm pitch. The focal length is different than in the previous case, so a linear motorized stage can place the relay lenses in such a way that the pixel scale remains constant at the detector. This setup can be used with fainter targets due to the smaller number of microlenses than the previous one.

A variety of wave-front reconstruction algorithms using data provided by SHS are available (Li & Jiang 2002). The modal reconstruction algorithm will be better in case of low signal-to-noise ratio (SNR) conditions (Li & Jiang 2002). For that reason we used the modal one for our project. In this procedure the measured focal position of each microlens is used to determine the local wave-front gradients, in such a way that the wave-front shape can be reconstructed by means of a vector of coefficients in a polynomial basis. The Karhunen-Loeve polynomials are used here.

The modal reconstruction algorithm is described in (Southwell 1980). Here we summarize the main steps of this procedure. The desired coefficient vector a , representing the reconstructed wave-front, can be derived from the array of measured wavefront gradients, by applying an inversion method:

$$a = (\mathbf{A}^\dagger \cdot \mathbf{A})^{-1} \mathbf{A}^\dagger \cdot \mathbf{S}, \quad (1)$$

where A is a rectangular matrix with $2N$ rows and M columns (with N being the number of microlens and M the total number of Karhunen-Loeve terms used). Its coefficients can be calculated from the partial deriva-

¹ <http://www.zemax.com>

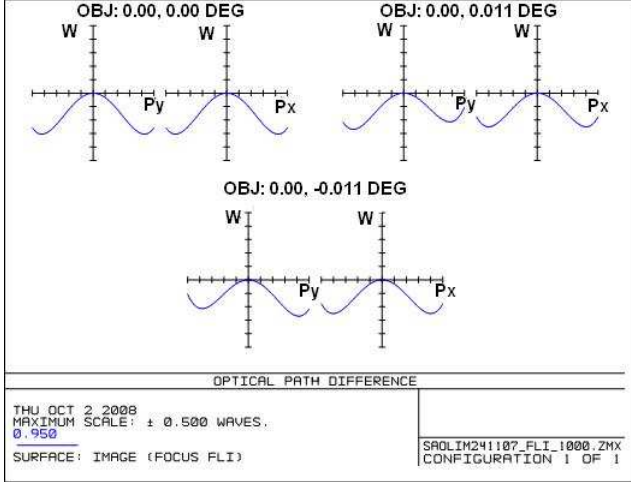


FIG. 5.— A ray fan diagram showing the aberrations of different angles (± 39.6 arcseconds) at the scientific camera of SAOLIM, estimated by Zemax.

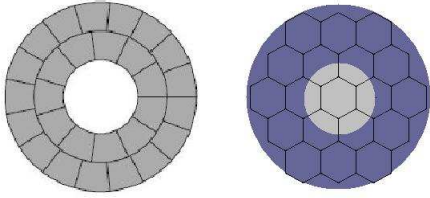


FIG. 6.— Left panel: Keystone-shaped lenslet array in 28 microlens configuration. Right panel: 5x5 lenslet array configuration. The blue area depicts the telescope pupil.

tives of the polynomials (Dai 1995). The local slopes can be organized to form a slope vector S of size $2N$ (Southwell 1980).

2.3. The Deformable and Tip-Tilt mirrors.

The micro-machined membrane deformable mirror consists of a chip with a silicon nitride membrane coated with aluminium. It was manufactured by OKO Technologies (Vdovin 1995). The membrane shape is driven electrostatically by the voltages applied to 39 control electrodes. Since the force between the membrane and the electrodes is attractive, the membrane can be pulled only toward its base. Therefore deformations in both directions can be led by biasing the mirror to a nonzero voltage. The reference value is 180 V for this bias, with an effective mirror diameter of 20mm according to the manufacturer.

The membrane is coated with an evaporated layer of aluminium to make it reflective and conductive. Two digital drivers provide an 8-bit voltage control for the output channels, whereas two high-voltage boards amplify the digital signals (0-250V) that are subsequently applied to each electrode.

The MDMM control is based on the previous knowledge of the so called influence functions. These functions are the responses of the membrane to the action of one particular isolated electrode. They were obtained by direct measurements of the wavefront, using the SHS system, when the highest voltage is applied to each actuator keeping the rest to the bias level

(Claflin & Bareket 1986). The surface’s wavefronts are expressed as a Karhunen-Loeve’s polynomial expansion with 14 terms (including the Tip-Tilt), which corresponds to the fourth order of these polynomials. The set of functions can be grouped into the so-called influence functions matrix (IFM). Assuming that the total deflection of the mirror is a linear superposition of the deflections resulting from each control channel, we can obtain the shape of the membrane as a response to a given set of voltages applied in the electrodes by a simple matrix multiplication:

$$IFM * V = a, \quad (2)$$

where vector V is the set of k squared voltages applied to each electrode and a is the shape of the membrane expressed in terms of an expansion of Karhunen-Loeve’s polynomials (Dai 1995):

The *control matrix* CM is obtained as the inverse matrix of IFM . It relates the vector of coefficients (S) to the required voltages by:

$$CM * S = V. \quad (3)$$

Because of the particular shape of the mirror, the CM is not a square matrix. Therefore a pseudo-inversion procedure to the IFM matrix is required in order to derive the CM . The Singular value decomposition method (SVD) was adopted. Some membrane modes may be removed by setting to zero a singular value in the IFM during the inversion process to avoid infinite values. This operation reduces the capability to reproduce some surfaces but it makes the control of the mirror more stable.

Finally, the procedure to create different surfaces or to compensate for the effects of the turbulence is applied iteratively. **The iterative process is a negative feedback loop and is similar to the one used by other AO systems (e.g. Hippler et al. 2000).** This allows us to obtain a better performance than with a single iteration, due to the non-linearity effects. Therefore the wavefront sensing errors or any overshooting in the applied voltages are minimized during this iterative operation (Closed-loop).

The set of 39 voltages V_n at instant n is given by

$$V_n = V_{n-1} + \alpha \cdot \omega(CM \cdot \phi), \quad (4)$$

where ϕ contains the SHS measurements of the wavefront shape expressed in terms of an expansion of the Karhunen-Loeve’s polynomials ($F_i(x, y)$) w is a vector of weights for each mode, and α is a damped parameter with values between 0 and 1. The finally adopted value for α was 0.75, derived empirically to grant the convergence of the iterative process. The surface generated with this set of voltages is the closest solution, in the least-squares sense, to the surface S . The root mean square (RMS) of the residual can be expressed by:

$$RMS = \left| \sum_i \phi_i F_i(x, y) - \sum_i \phi'_i F_i(x, y) \right|. \quad (5)$$

Therefore,

$$RMS = \left| \sum_i (\phi_i - \phi'_i) F_i(x, y) \right| = \sqrt{(\phi_i - \phi'_i)^2}. \quad (6)$$

The Tip-Tilt can be compensated with the deformable mirror, at the expense of consuming a substantial fraction of the dynamic range of the actuators. As an alternative solution, a steering mirror is used for that purpose.

The Tip-Tilt mirror was manufactured by SBIG². It consists of a steering mirror capable of achieving motion rates up to 50Hz. This Tip-Tilt mirror has magnets on the back size. That interact with the current flowing through a set of voice coils on the housing module to rapidly move the mirror. The technique is very similar to that employed in loudspeakers, except that there the magnet is fixed and the wires are on the speaker cone. The mirror and magnets are suspended using a flexible beryllium copper membrane. A needle pushes up against a jewel bearing mounted at the center of the mirror to hold the focus constant. SBIG has developed a proprietary technique to rapidly damp the motion of the mirror, so small movements are precise, with very little overshoot or fluctuations. The tilt of the mirror during operation is very small, and it does not lead to any measurable de-focus at the edges of the frame. The correction range of the Tip-Tilt mirror is about ± 250 microns **that represents approximately 10 arcseconds on the sky, which is enough for the application. An specific 50Hz algorithm is used for the tip-tilt mirror. The telescope is tracking at sidereal rate but we do not autoguide on off-axis guide stars.**

3. INSTRUMENT CONTROL

3.1. Instrument control electronics.

SAOLIM is operated by a remote control without direct human interaction with the instrument. This control electronics were designed to contain all the sub-systems and there were packed into a single electronic rack located just below the optical bench. Everything is mounted in a rigid custom-designed aluminium frame. It contains the following major components: a Pentium IV 3.4Ghz PC as master hardware controller, a DM Electronics with DC and high voltage amplifiers, a Tip-Tilt mirror controller, some steeper motor controllers, shutter controllers, different power supplies, and a miscellaneous of support and auxiliary electronic units. The amount of dissipated heat is negligible with no effect at the optical bench. However, two fans remove the air inside the electronic rack. **They do not cause detectable vibrations.** A liquid-cooled heat exchanger is installed in this level to remove the heat produced by the EMCCD inside the optical bench. This allows us to turn off its fan during the observations at the telescope, avoiding potential turbulences in the optical path.

The following motorized functions are served by different electronics sub-systems: a control unit of the SHS shutter, a linear stage to focus the relay lens onto the SHS, a filter exchange stage for SHS, and a Tip and Tilt stage of the folding mirror, E8 in Figure 1, and finally a linear stage to place the white reference fiber in the optical path.

The PC control is connected via Ethernet through a router providing direct access from any terminal. A wireless connection is also available. Such wireless connection is very convenient when the instrument is controlled next to the telescope for diagnostics purposes.

² <http://www.sbig.com>

3.2. Instrument control software.

The system is operated under a Windows XP operating system. **Thanks to the very fast processors of modern PCs, all the procedures can be run under such operating system, without detectable speed losses. Its use is a new approach and a novelty which reduces hardware costs considerably.** The control software is written in Microsoft Visual C++ providing enough computation power for the reconstruction algorithms and shielding the user from the detail knowledge of the device parameters.

3.3. Scientific camera.

All the tests presented in this article were done using a non-optimal 1kx1k back-illuminated CCD camera. By the time of development of the instrument, we did not have access to a more adequate detector, like a NIR camera, which is the usual scientific camera in other AO systems. This camera was used only for testing purposes to check the goodness of the operation of the reconstruction algorithms. Therefore, no scientifically useful data were obtained at this stage. All the observations were performed in the very near infrared regime, using a narrow-band filter with a central wavelength of 1033nm and a bandwidth of 10nm. **The transmission was measured and it has no blue leaks.** At this wavelength range, the camera has still $\sim 5\%$ quantum efficiency, (QE). For that reason, only bright stars could be observed. This will not hamper the results presented here, since our main goal was the test of the design and construction, not to produce scientifically useful data at this point.

In a second future stage, a fast frame rate EMCCD camera is intended to replace the current scientific camera.

4. PERFORMANCE OF THE INSTRUMENT.

4.1. Mechanical stability of the prototype.

The mechanical design of the instrument is provided by a solid aluminium cast housing, which keeps all the optical elements in place. During some bad weather nights, flexure tests at the telescope were performed. The telescope was pointed to different positions in hour angle and declination. At each position, the reference fiber pattern was recorded at the Shack-Hartmann sensor which computes the resulting Tip and Tilt values of the image. As a result, flexures of the instrument were determined to be negligible at any location. Their maximum value was ~ 0.5 arcsec at 30 degrees of telescope elevation pointing to the south. In addition, the motorized stages were tested at very low telescope elevations showing an acceptable behavior, reproducing the same available positions.

4.2. Sensitivity of the WFS.

One innovative aspect in the SHS design was the use of an EMCCD as a detector. This pioneering camera has had a profound influence on photon starved imaging applications, as photon counting in astronomy (e.g. Dussault & Hoess 2004). The back-illuminated device combines photon collection efficiencies of up to 95% QE with single photon sensitivity through the virtual elimination of the readout noise. **It is likely that some**

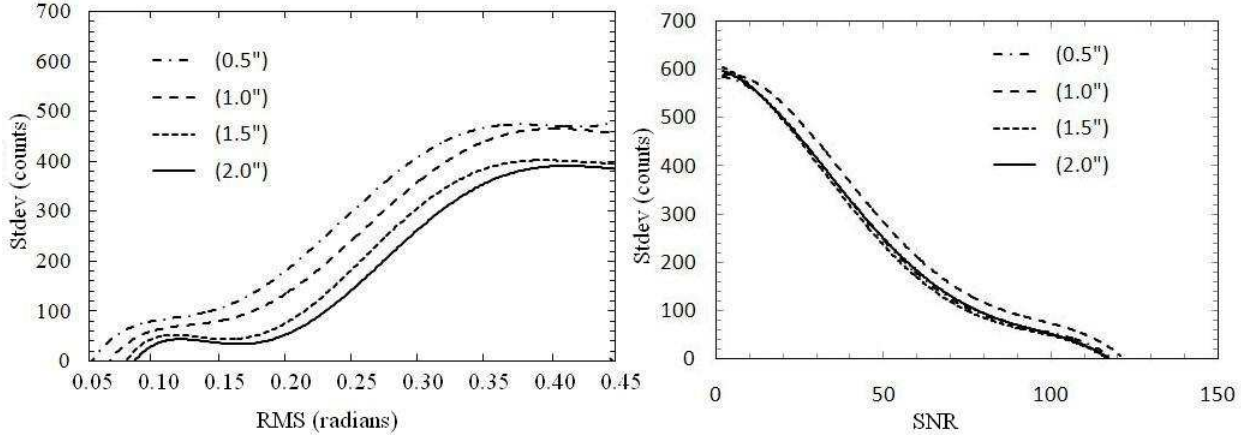


FIG. 7.— Left panel: RMS of the wavefront reconstruction measured with SHS versus Standard deviation for different seeing conditions. Units of RMS are in radians. Right panel: SNR per lenslet channel measured with SHS versus standard deviation for different seeing conditions. In that case, all the plots are very similar because the photometric aperture was constant and bigger than the simulated seeing value.

TABLE 2
SENSITIVITY MEASUREMENTS OF SHS. AVERAGE SEEING
FWHM 1.3''-1.6''. CAMPAIGN 03-07-2008.

Star Name	m_v	Total Flux.	SNR ^a	EMCCD Setup
HR7315	5.3	136785	187.7	EMGain=100, Freq=135Hz
HD171827	7.7	61428	128.7	EMGain=210, Freq=103Hz
SAO67491	8.6	10944	52.9	EMGain=210, Freq=103Hz
SAO68044	9.7	4213	38.5	EMGain=210, Freq=103Hz
PPM82785	10.7	956	19.1	EMGain=255, Freq=103Hz
GSC2662	11.8	192	7.5	EMGain=255, Freq=103Hz

^a(Robbins & Hadwen 2003)

fake detections may arise. Their effect will be to increase the net rms of the reconstructed wavefront. For that reason, the final performance of the instrument has to be measured on real stars.

During the commissioning of the instrument, in the observing period of 2008, a set of stars with different brightness were observed to estimate the overall sensitivity of the instrument. The results are summarized in Table 2. The photometry was performed by using a circular aperture of 6 pixels using the DAOPHOT package of IRAF. The table shows the star name, V-band magnitude, total flux in counts and signal-to-noise ratio (SNR). Each measured parameter in the table represents the average value over all the sub-apertures. All the images were corrected for dark current and pixel-to-pixel variations. The table shows the detection limit of the instrument, which is defined as the maximum magnitude at which the control software is able to compute a centroid for every subaperture of the lenslet array and keep close-loop operation. Such limit is 11.8 mag for SAOLIM. This detection limit is similar to that one of more complex and expensive AO systems, like ALFA, mounted at the 3.5m telescope of the Calar Alto observatory), which was able to use stars as faints as $V \sim 12$ to close the loop (Hippler et al. 2000).

An empirical relationship between the SNR per sub-

aperture measured by the SHS and the star brightness can be established by an exponential fitting to both parameters, yielding:

$$SNR = 9538.6_{\pm 1.6} e^{-0.4657 \pm 0.015 m_v} \quad (7)$$

in that way, the expected SNR can be estimated for any magnitude. The accuracy of the centroid algorithm during the wavefront reconstruction is determined by the SNR per sub-aperture. Therefore, some experiments have to be performed with the aim to predict the capability of the system to compensate a turbulence under different seeing conditions and different star magnitudes.

To do so, a reference fiber is fed with a white source and it was placed exactly at the focal plane of the telescope, simulating a perfect reference star. By adding white noise to the whole image in steps of 0.5 counts, the RMS (eq 6) and the SNR can be measured as a function of the noise on the different images recorded by the SHS. Finally, a relation between them can be established. This procedure was repeated until the SNR dropped to a low value (~ 10), when the uncertainty of the centroid coordinates was high. Moreover, different seeing conditions were simulated by convolving the reference fiber pattern image with a Gaussian function with different widths. In total, 4000 realizations of the RMS and the SNR vs the standard deviation of the input noise were performed for this simulation. An empirical relation between the input standard deviation of the simulated noise, and the output RMS of the reconstructed image and the final SNR of the detected sub-images was derived for each input seeing by fitting the simulated data sets with a 5th order polynomial function, for each pair of parameters. The simulations are shown in Figure 7.

As a result of the former simulations, the Strehl ratio (at $\lambda = 550\text{nm}$) can be derived and related to the V magnitude as shown in Figure 8. Therefore, the faintest star that can be used as reference by SAOLIM to compensate the turbulence should have a brightness of at least $V \sim 11.5$ with the 28 microlens array. **This value was obtained for a natural seeing FWHM of 1 arcsecond** ($r_0 = 10\text{cm}$). The final accuracy of the correction will

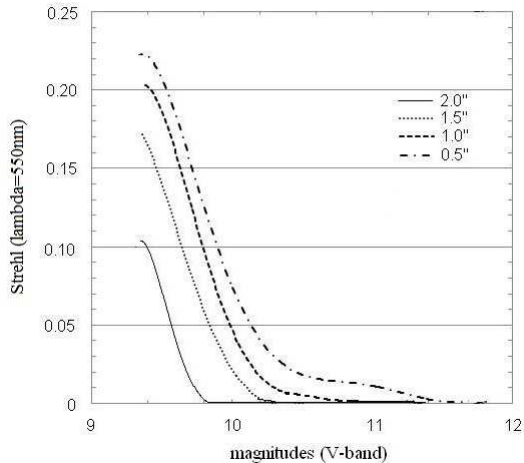


FIG. 8.— **Simulated** relation between the Strehl ratio and V magnitude measured by SHS for different seeing conditions.

TABLE 3
TECHNICAL RUNS FOR THE COMMISSIONING OF SAOLIM DURING 2007 AND 2008 IN THE OBSERVATORY OF CALAR ALTO OBSERVATORY.

Date	Goals
(2-5)-07-2007	Determination of the pixel scale. Flexures. Wavefront sensitivity.
(28-30)-09-2007	First image obtained on the scientific camera of a real star with the Tip Tilt compensation.
(11-14)-05-2008	First images obtained on the scientific camera of a real star with the high order compensation (under very bad seeing conditions, performance from 2.5'' to 1.2'').
16-08-2008	Evaluation of the performance of the high order loop on the scientific camera under average seeing condition.

depend strongly on the input natural seeing conditions.

5. RESULTS ON THE SKY.

Four technical campaigns were carried out to test the performance of the instrument on real stars at the 2.2m telescope of the Calar Alto observatory. The goals for these observing runs are summarized in the Table 3.

5.1. Static aberrations of the telescope.

The static aberrations of the 2.2m telescope are well known (U. Thiele private communications). They were analyzed previously by using the intra-extra focal images technique (van Dam & Lane 2002). This method provides a set of Zernike coefficients that characterizes those aberrations. To check the reliability of the reconstruction algorithm adopted in SAOLIM, a routine was implemented in the control software to determine them. For doing so, the routine computes the wavefront coefficients of 10000 images. Under good seeing conditions

TABLE 4
COMPARISON BETWEEN STATIC COEFFICIENTS OF THE 2.2M TELESCOPE AT CALAR ALTO OBTAINED WITH THE INTRA-EXTRA FOCAL IMAGES AND SAOLIM WAVEFRONT SENSOR.

Aberration	RMS CAHA(nm)	RMS SAOLIM (nm)
Astigmatism (sin)	-7.54	-6.5±1.0
Astigmatism (cos)	21.2	22.2±1.0
Coma (sin)	5.36	4.3±0.6
Coma (cos)	8.42	10.1±0.5
Trifoil (sin)	4.81	3.7±0.6
Trifoil (cos)	5.21	5.8±0.5
Spherical	13.1	12.9±0.3
Quad astig (sin)	-0.50	-0.6±0.3
Quad astig (cos)	-2.02	-2.5±0.3

the mean values of the coefficients represent the static aberrations of the telescope. Table 4 lists the coefficients of the static aberration of the telescope measured by the method described before. There is a very good agreement between both estimations showing the capability of the instrument to analyze correctly the turbulence aberrations.

5.2. The Tip-Tilt algorithm on a real star.

In order to test the Tip-Tilt compensation algorithm a real star (HR7331) was observed under average seeing FWHM of 1.3''. The star was not centered on the detector on purpose. The drift of the centroids imaged by the lenslet array with respect to a reference image produced by a fiber placed at the focal plane of the telescope, are computed by the wavefront sensor. With a proper calibration, the Tip-Tilt mirror is commanded in such a way that the drift is minimized in both axes.

Figure 9 shows the variations of the centroid of the star. They are minimized when the compensation is imposed in such a way that the standard deviation of the measurements decreases from 0.27 to 0.16 pixels. Besides this, the star is brought to the center of the SHS by the system. An improvement of 25% in terms of the FWHM and of 40% in terms of peak intensity is measured on the scientific camera as shown in Figure 10.

5.3. High order closed-loop results.

The high order algorithm (HO) was also tested with real observations on the sky. The test comprises the measurements of the *RMS* of the wavefront (eq.6) during the open-loop and the closed-loop procedures. In the ideal case, this magnitude should be zero when the wavefront compensation is active which will mean that the wavefront is flat. In the closed-loop operation when the SHS only measures the residual image motion after each correction, the measured values are smaller, than in open loop operation.

Figure 11 shows the *RMS* measured by the wavefront sensor during the open-loop procedure, the Tip-Tilt and the high order compensation procedures as a test to check the smooth performance of the reconstruction algorithms. Again, the units are radians. Clear differences between the three processes are appreciated. A natural

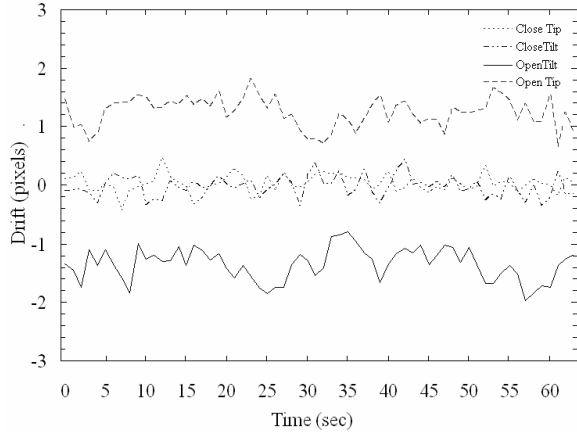


FIG. 9.— Centroid distances of the SH star pattern with respect to the SH reference fiber when a Tip-Tilt compensation is applied.

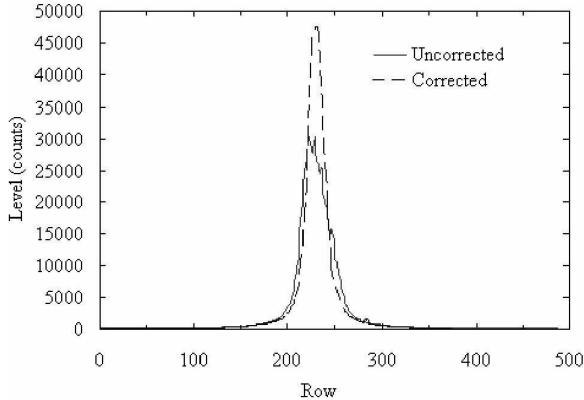


FIG. 10.— Horizontal intensity cut of HR7331 image on the scientific camera. An improvement of 25% in FWHM and 40% in peak intensity is observed when the Tip-Tilt compensation is applied. The natural seeing FWHM was about $1.3''$. Corrected seeing FWHM was $1.02''$.

guide star of $V \sim 5.2$ magnitude was used for this experiment, with a SHS frame rate of 420Hz and collecting a total number of 21000 counts for each process. The average seeing FWHM conditions were around $1.4''$. An improvement of a factor $\sim 2 - 3$ is observed in terms of measured *RMS* by the Shack-Hartman sensor when only the Tip-Tilt compensation (TT) is applied. When the high order algorithm (HO) is added, a decrease of the *RMS* by a factor 15 is seen. On the other hand, a decrease in the median values of every mode's coefficient is observed. The decrease for the modes from 2-10 is listed in Table 5.

Any AO system may have internal inconsistencies: i.e., the system considers that the correction is adequate, minimizing the *RMS*, but the wavefront is not correctly compensated. For instance, this may happen if the wavefront sensor has a systematic error. Then the influence functions for the membrane would be obtained with that bias, and the global failure of the system would not be noticeable only from the analysis of the *RMS*.

To be completely sure of the performance of our AO system, simultaneous images were taken with the scientific camera. Figures 12-14 show some examples of

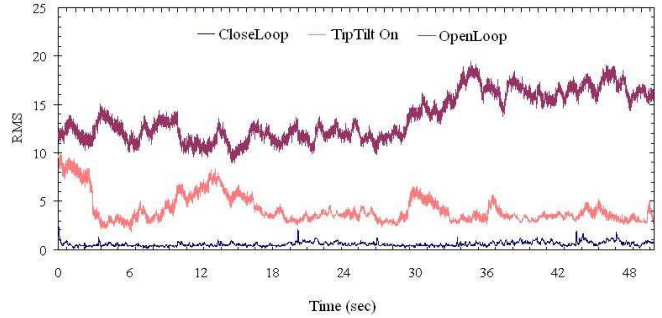


FIG. 11.— *RMS* of the wavefront during Open-Loop, Close-TT and Closed-Loop for a real natural star. Units are given in radians for $D/r_0 = 22$.

TABLE 5
COEFFICIENTS OF THE MODES 2-10 WITH AND WITHOUT HO COMPENSATION. VALUES ARE IN MICRONS.

mode	Open-loop	HO+TT
2	2.59	0.015
3	0.96	0.002
4	-0.45	-0.011
5	-0.41	-0.002
6	0.13	-0.006
7	-1.33	-0.14
8	-0.05	0.11
9	-0.17	-0.08
10	0.22	0.21
Average	1.04	0.09

a real-time closed-loop aberration compensation using a natural guide star. These preliminary results were obtained during the commissioning of the instrument at the 2.2m Calar Alto telescope. An observing log of the observations carried out can be found in table 6.

The images are clearly improved when applying the closed loop wavefront compensation even under quite poor seeing conditions. Figure 12 shows a 4.6 magnitude star (SAO88071) observed under very bad turbulence conditions, with a natural seeing FWHM of about $2.5''$. The data were obtained during the campaign of May 2008. Under such bad seeing, 30% of the actuators reached their maximum values and therefore only an improvement of a factor of 2 in terms of FWHM could be achieved. The central wavelength of the observations was again the same as before. The frame rate of the reconstruction was 420Hz and 14 modes were taken into account with the KS28 lenslet array. Under these poor observational conditions, observing techniques like lucky imaging are completely useless. However SAOLIM was able to reduce the FWHM of the output image to half of its input value and to increase the peak intensity by a factor ~ 6 . Figure 13 illustrates that correction. Since the lucky imaging technique is feasible with an input seeing FWHM of $\sim 1''$ (Hormuth et al. 2008), this experiment demonstrates how our instrument can improve the performance of a lucky imaging device.

During the campaign of September 2008, the system was tested under better seeing conditions. In the left panel of Figure 14, an image of the double star WDS01095+4795 (with a visual magnitude of 4.59 and

TABLE 6

OBSERVING LOG FOR SOME OF THE RESULTS OBTAINED WITH THE SCIENTIFIC CAMERA OF SAOLIM DURING THE OBSERVING RUN AT THE TELESCOPE. A NARROW BAND FILTER (1033/10NM) WAS USED DURING ALL THE OBSERVATIONS.

Date	UT	Objectname	V mag	Exp. Time	Loop parameters	FWHM _{Uncorrected}	FWHM _{Corrected}
2008-05-13	02:00	SAO88071	4.6	10 sec	420Hz 14 modes	2.5"	1.2"
2008-09-16	19:46	SAO103052	6.2	10 sec	420Hz 16 modes	1.2"	0.37"
2008-09-17	02:40	WDS01095+4795	4.59 and 5.61	10 sec	300Hz 16 modes	1.1"	0.32"



FIG. 12.— Left panel: Image of the star SAO88071 taken with the scientific camera of SAOLIM during openloop. Both images are a subwindow of 4×4 arcsec. Natural seeing FWHM was 2.5 arcseconds. Right panel: Same star under same seeing conditions during closed loop procedure. Corrected seeing FWHM was 1.2 arcseconds. The images were taken with a narrow filter with a central wavelength of 1033nm and 10nm of bandwidth from the Calar Alto 2.2m telescope. The reference star has a 4.66 V-band magnitude.

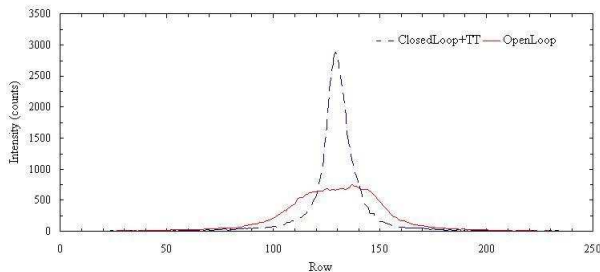


FIG. 13.— Intensity profiles of the open and closed loop images shown in Fig 12.

5.61) is shown, taken with SAOLIM, without applying any corrections. The natural seeing FWHM was $1.1''$ during the observations. The separation of the star is $0.4''$ hence it was unresolved and appeared as a single spot in the image. The right panel shows the same object observed with the real-time closed-loop active. The corrected FWHM was $0.32''$ and as a result of this, the double star is clearly resolved. The frame rate of the loop was 300 Hz.

This result is quite promising if the prototype is attached to a lucky imaging camera. When combined with an AO system, Lucky Imaging selects the periods when the turbulence that the adaptive optics system must correct is reduced. In these periods, lasting a small fraction of a second, the correction given by the AO system is sufficient to give excellent resolution with visible light. The Lucky Imaging system sums the images taken during the excellent periods to produce a final image with much higher resolution than is possible with a conventional long-exposure AO camera (Law et al. 2006).

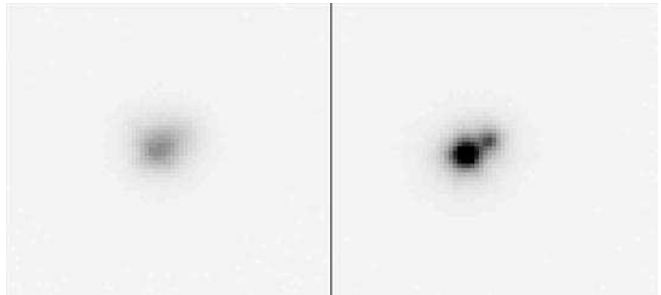


FIG. 14.— Images of the double star WDS01095+4795 of 4.59 and 5.61 magnitudes respectively taken with the scientific camera of SAOLIM. Both images are a subwindow of 4 arcsec². Left panel: Open loop. Right panel: Closed loop. The loop frequency was 300Hz and 16 modes were corrected. The double star has a separation of 0.4 arcsec and it is perfectly resolved. The central wavelength of the observations was 1033/10nm. Both images are displayed with the same cut levels. Natural seeing FWHM was 1.1 arcsec and the corrected one was 0.32 arcsec. The peak intensity rose up from 2300 to 10200 counts.

6. CONCLUSIONS

A low cost adaptive optic system was developed for astronomy and tested. It uses a 39-actuator membrane deformable mirror of 20mm diameter, a fast frame rate EMCCD as detector of the wavefront sensor and a low cost Tip-Tilt mirror. The whole prototype is running in a single PC, resulting in a compact module easy-to-install and transport with a total weight of only 70kg. Experimental simulations were carried out to determine the sensitivity of the wfs and to predict the limit magnitude of the star to be used. This limit was found to be 11.5 magnitudes. The system was made up of entirely commercial hardware components with a total cost of about 35000 euros. We did not count here **the manpower costs**.

A powerful method was adopted to evaluate the capabilities of a membrane deformable mirror to produce and correct different aberrations within the range of interest in astronomy. This is a general approach, suitable for use in every system whose control was based on a previous knowledge of its influence functions. Under the assumption of linearity, the proposed iterative algorithm works with the required precision, making it appropriate to use in real-time applications. Karhunen-Loeve's polynomial or any arbitrary surface could be reproduced when this procedure is systematically applied, taking into account the available range of voltages of the mirror. A real-time (up to 420Hz) closed-loop algorithm has been incorporated to the device for the compensation of atmospheric turbulence.

The system has been tested on real stars. The best

images obtained had a FWHM of 0.32 arcsec from an input natural seeing FWHM of 1.1 arcsec. Although the system does not achieve diffraction limited images, the FWHM is improved by a factor of 4. Under quite poor seeing conditions (FWHM=2.5") 30% of the DM actuators were saturated, but an improvement of a factor of 2 was measured in the FWHM of the images. The Tip-Tilt mirror showed a good behavior too reducing the FWHM from 1.3" to 1.02".

The use of this AO system attached to a Lucky imaging system could enhance the spatial resolution of the input images and the fraction of useful images, and therefore the performance of such a system will be increased. Both techniques will be tested in the future.

We are grateful to Plan nacional I+D+I de Astronomia y Astrofísica AYA2005-07808-C03-01 and AYA2008-

06202-C03-01 that supported this project. Also FEDER funds are acknowledged. The authors are grateful to the Plan Andaluz de Investigación, Desarrollo e Innovación, who granted this study under the projects: P08-FWM-04319 and FQM360. They would also thank the ICTS-2009-32 program of the Spanish Ministerio de Ciencia e Innovación. The paper is based on observations collected at the Centro Astronómico Hispano Alemán (CAHA) at Calar Alto, operated jointly by the Max-Planck Institut für Astronomie and the Instituto de Astrofísica de Andalucía (CSIC). We are grateful to Luzma María Montoya and Santos Pedraz for their help during the observations. We would like to thank the anonymous referee for the useful comments.

SFS would like to thank the *Fundación Agencia Aragonesa para la Investigación y el Desarrollo* (ARAID), for the financial support during the last year.

REFERENCES

- Bates, R. H. T.; Cady, F. M. 1980, *Opt. Commun.*, 32, 365
 Claffin, E. S.; Bareket, N. J. *Opt. Soc. Am. A*3, 1833-1840.
 Dai, G. M., 1995, *JOSA A*, 12 pag 2182-2193
 Dainty, J. C., Munro, I., Patterson, C., & Wooder, N. J. 1999, *Proc. SPIE*, 3749, 721
 Dussault, D., & Hoess, P. 2004 *Proc. SPIE*, 5563, 195
 Hippler, S., et al. 2000, *Proc. SPIE*, 4007, 41
 Peter, D., Feldt, M., Henning, T., Hippler, S., Aceituno, J., Montoya, L., Costa, J., & Dorner, B. 2010, *PASP*, 122, 63
 Hormuth, F., Hippler, S., Brandner, W., Wagner, K., & Henning, T. 2008, *Proc. SPIE*, 7014
 Law, N. M., Dekany, R. G., Mackay, C. D., Moore, A. M., Britton, M. C., & Velur, V. 2008, *Proc. SPIE*, 7015
 Law, N. M., Mackay, C. D., & Baldwin, J. E. 2006, *A&A*, 446, 739
 Li, X., & Jiang, W. 2002, *Proc. SPIE*, 4825, 121
 Kasper, M. E., & Hippler, S. 2003, *Proc. SPIE*, 4839, 266
 Paterson, C., Munro, I. H., & Dainty, C. 2000, *Proc. SPIE*, 4007, 185
 Southwell, W. H., 1980. *J. Opt. Soc. Am.* 70, 998-1006
 van Dam, M. A., & Lane, R. G. 2002, *Proc. SPIE*, 4825, 237
 Vdovin, G. 1995, *Applied optics*, 34, 2968-2972.
 Robbins, M. S.; Hadwen, B. J. 2003, *IEEE Transactions on Electron Devices*, 50, 1227-1232.